

Nicholas G. Paulter Jr.,¹ Donald R. Larson,² and John A. Ely³

Handheld Metal Detector Characterization Using Spherical Test Objects

Reference

N. G. Paulter Jr., D. R. Larson, and J. A. Ely, "Handheld Metal Detector Characterization Using Spherical Test Objects," *Journal of Testing and Evaluation* 48, no. 2 (March/April 2020): 1262–1276. <https://doi.org/10.1520/JTE20170339>

ABSTRACT

The detection performance of handheld and hand-worn metal detectors is based on observing an alarm indication from the metal detector when a test object is brought near the metal detector. These test objects maybe actual threat items or simulated threat items. The detectability of the test object is dependent on the electromagnetic properties of the test object, its shape and size, and its orientation relative to the magnetic field generated by the metal detector. Small misorientations of a test object, relative to a reference orientation, may cause the operator to incorrectly attribute a higher performance to the metal detector than it can provide. Consequently, to support accurate and reproducible characterization of the performance of a metal detector, orientation effects should be minimized or eliminated. Spherical test objects are presented to eliminate these effects for handheld and hand-worn metal detector performance assessments.

Keywords

detection performance standard, detection response, handheld metal detector, hand-worn metal detector, magnetic field, baseline performance, object orientation, test objects

Introduction

Handheld metal detectors (HHMDs) and hand-worn metal detectors (HWMDs) work by generating an alternating magnetic field that interacts with nearby objects that are electrically conductive or magnetically permeable or both and then sensing the effect of that interaction. HHMDs are ubiquitous in security screening of metal threat objects and contraband. The HWMD is a relatively new instantiation of security screening metal detector

Manuscript received June 13, 2017; accepted for publication April 17, 2018; published online September 12, 2018. Issue published March 1, 2020.

¹ National Institute of Standards and Technology, 100 Bureau Dr., Gaithersburg, MD 20899, USA (Corresponding author), e-mail: nicholas.paulter@nist.gov, <https://orcid.org/0000-0002-9782-0894>

² Entegra Corporation, 22057 E. Easter Cr., Aurora, CO 80016, USA, <https://orcid.org/0000-0003-4395-8684>

³ National Institute of Standards and Technology, 100 Bureau Dr., Gaithersburg, MD 20899, USA

but is gaining popularity because it frees the operator's hand for other purposes. The HWMD is typically operated with the sensor within a couple of millimeters from the surface being searched, whereas the HHMD is nominally held 1 cm to 2 cm from the surface being scanned, depending on the intent of the search.

The detection performance of HHMDs and HWMDs is tested by bringing a metal test object (the exemplar) near the metal detector and noting an alarm indication. These exemplars are often an actual threat object, but this is not ideal because (a) the design or manufacture of an actual threat object may change, unbeknownst to the operator, and thus change the apparent sensitivity of a metal detector to that threat object, and (b) the detectability of threat objects and their exemplars are dependent on their orientation relative to the metal detector. The exemplars have several purposes: (a) in the assessment of the performance of a given model of metal detector, (b) in support of the historical comparison of the performance of a given metal detector or model of metal detectors, (c) in support of product comparison, and (d) to establish baseline performance of a technology (like an HHMD). If the exemplar varies with time because of manufacturing or design change or the detection results are subject to significant uncertainty, then none of these purposes can be fulfilled accurately or reproducibly. To achieve these purposes, the exemplar should have well-defined geometries and material characteristics, with appropriate tolerances. It would not necessarily need to look like an actual threat object. Such exemplars allow more consistent comparative evaluation of the performance of metal detectors than will actual threat objects and, if appropriately designed, would be the basis of a minimally acceptable performance requirement for a metal detector.

Baseline performance describes the broadest and most common performance requirements. It is not the most rigorous or strict detection performance but establishes the minimum performance below which a model is not considered for more exhaustive or more specific threat detection testing. For a general metal detector performance standard, which is the goal of our work, baseline performance is the logical approach. The other approach would require testing for unique set of requirements that will be unique for each agency and for a given period of time. This specific testing is necessary for an agency to accept a model for procurement and requires detailed knowledge of the changing threats. Baseline-performance testing can foster an expedient agency-specific testing program.

Spherical test objects support these purposes because their detectability is orientation independent, they can be readily fabricated and procured having a fixed composition and diameter, and they can be designed to have the same nominal electromagnetic response as that of actual threat items at given orientations. Spherical test objects greatly reduce measurement uncertainty and, consequently, provide a more accurate and reproducible measure of the detection performance of the HHMD and the HWMD than can testing with threat-object exemplars.

Measurement Uncertainties

The measurement uncertainty, u_{meas} , of the signal produced by the metal detector in response to a metal object can be described by the following Eq 1:

$$u_{meas} = \sqrt{u_{inst}^2 + u_{R\&R}^2 + u_{exmplr}^2}, \quad (1)$$

where u_{inst} is the instrumental measurement uncertainty (including analyses and computational methods), $u_{R\&R}$ is the uncertainty for reproducibility and repeatability, and u_{exmplr} are the measurement uncertainties associated with the exemplar, which is given by [1]:

$$u_{exmplr} = \sqrt{u_{prpty}^2 + u_{geom}^2 + u_{orient}^2}, \quad (2)$$

where u_{prpty} is the measurement uncertainty associated with the electrical conductivity, σ , and magnetic permeability, μ , of the test object; u_{geom} is the uncertainty for the physical dimensions of the test object; and u_{orient} is the uncertainty associated with the orientation of the test object relative to the metal detector under test.

The focus of this article is on u_{orient} , which can be described using the method of linear propagation of uncertainties (LPU) [2]:

$$u_{orient} = \sqrt{u_{xmp/blk}^2 + u_{blk/hldr1}^2 + u_{hldr1/rob}^2 + u_{rob/hldr2}^2 + u_{hldr2/dctr}^2 + \sigma_{\theta}^2}, \quad (3)$$

where $u_{xmp/blk}$ is the uncertainty in the orientation of a reference plane or position on the exemplar relative to a reference plane on the block, where the block is used to contain the exemplar; $u_{blk/hldr1}$ is the uncertainty in the orientation of the block relative to the block holder, where the block holder is a device that secures the block to the robotic or manual positioning instrument; $u_{hldr1/rob}$ is the uncertainty in the orientation of the block holder relative to the robotic instrument to which it is attached; $u_{rob/hldr2}$ is the uncertainty in the orientation of the robotic instrument relative to the detector holder, where the detector holder is attached to the robotic instrument; $u_{hldr2/dctr}$ is the uncertainty in the orientation of a reference plane of the detector holder relative to a reference plane on the metal detector; and σ_{θ} is the standard deviation of the angular variation of the orientation of the outer surface of the metal detector relative to the plane of the detector coil. In the LPU given in Eq 3, it is assumed that the variation in all the parameters is normally distributed and that the measurement uncertainty contributors are derived from many independent measurements. Ref. [1] provides more information on these uncertainties.

Numerical Simulation of the Interaction of the Exemplar with the Magnetic Field of the Metal Detector

Ref. [1] provides detailed information on the electromagnetic field simulations that were used to compare the inductive coupling of an exemplar to an idealized circular coil, which, when energized, is the source of the magnetic field that interacts with nearby objects. A manufacturer has different options, many proprietary, for measuring and processing the signal representative of the inductive coupling between their metal detector and a metal object. Therefore, because of the likely departure of a simulated circuit design from a manufacturer's proprietary designs and software, only the magnitude of the inductive coupling itself was simulated in [1]. The simulations were experimentally validated here for certain metal detector operational and design parameters using a custom circuit (see "Experimental Validation of the Numerical Simulations").

Examples of the possible unique orthogonal orientations of the knife exemplar (a simple rectangular prism) relative to the coil are shown in Fig. 1. Each of these orthogonal orientations are arranged such that one surface of the test object is parallel to the plane

FIG. 1

The possible unique orthogonal orientations of a thin rectangular prism that can be presented to a metal detector, which is represented by a loop. The white arrows show the direction of motion of the test object relative to the loop.

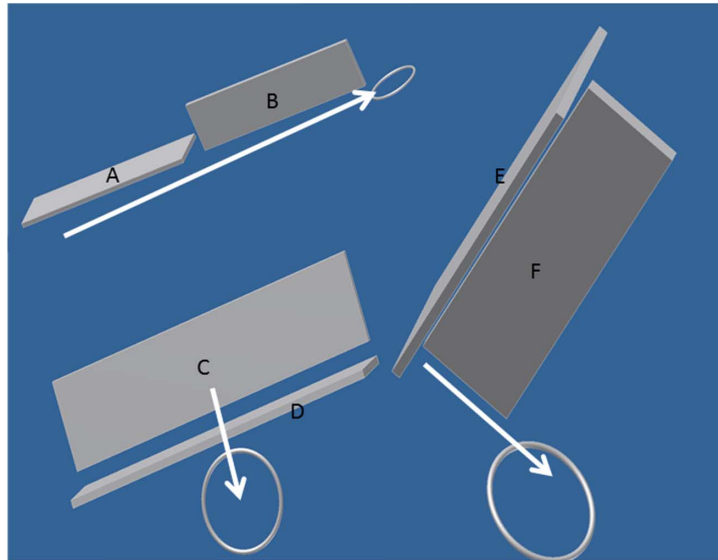


TABLE 1

The relative coupling of a knife exemplar for the orientations shown in Fig. 1, with Orientation C as the reference. The values were obtained using electromagnetic simulation.

Orientation	A	B	C	D	E	F
Relative coupling	0.6777	0.0919	1.000	0.1284	0.1464	0.0517

of the coil. The separation between the coil and the surface closest to the plane of the coil was fixed, as this represents actual use. The relative orientation-dependent coupling values are given in Table 1.

Fig. 2 shows the results of the simulation for the nonferromagnetic threat-based exemplars and the spheres [1]. Ref. [1] also contains simulation information for ferromagnetic threat-based exemplars. The simulations' results were consistent with previously published results for similar geometries [3–5].

Experimental Validation of the Numerical Simulations

The exemplars (see Table 2) were approximate replicas of a gun (fabricated from steel, aluminum, and zinc), knife (steel, aluminum, and nonferromagnetic stainless steel), handcuff key, screwdriver bit, razor blade, 22 caliber cartridge, and pen refill, and are described in detail in Ref. [1]. These exemplars are those developed by the National Institute of Standards and Technology (NIST) for the National Institute of Justice Standard 0602.02, *Hand-Held Metal Detectors for Use in Concealed Weapon and Contraband Detection* [6]. Only two orientations of the threat object exemplar were used: one that produces the maximum detection sensitivity, and the other that produces the minimum detection sensitivity. For the knife exemplar, these orientations are labeled C and F in Fig. 1.

were designed to emulate the extreme range of the coils found in commonly used HHMDs. The oscillation frequencies that were used in this study were determined by the coil inductance and the observed range of oscillation frequencies generated by commonly used HHMDs. The frequency of the generated magnetic field was recorded by the frequency counter. When a test object was brought near the coil, the inductance changed, and the resulting change in resonant frequency of the LC tank circuit were recorded. Care was exercised to limit the contributions of other, nearby objects (human body parts, tables, and other supports) to the measurement results.

Two frequencies (5 kHz and 1 MHz) and two coil geometries (120-mm-by-20-mm rectangular coil and 120-mm-diameter coil) were selected, as they represented the extremes for the commonly used HHMDs. Four coils were fabricated, two for each geometry with different number of wire loops, as this was necessary to obtain operation at the two different frequencies. A fifth coil with an inside diameter of 20 mm and operating at approximately 50 kHz was also used. This coil diameter and frequency were selected for comparison with the numerical simulations performed in [1]. For the LC tank circuit, the resonant frequency, f , is related to the inductance, L , and the capacitance, C , by the following equation:

$$f = \frac{1}{2\pi\sqrt{LC}} \tag{4}$$

The measurement procedure consisted of making a reference measurement that did not have an exemplar present and then making another measurement with an exemplar present. The difference between the two results was then calculated. In each case, the exemplar or coil was positioned to maximize the change in frequency and thus inductance. This procedure permits the measurements to be relative and cancels drift. Each measurement was repeated ten times, and the mean and standard deviation were calculated. A plastic barrier that is approximately 1-mm thick was positioned between the coil and the exemplar to maintain a constant separation between them.

The measurement results for the four coils appear in [Tables 3 and 4](#). Shown is the sphere diameter that provides a coupling value that most closely matches the coupling

TABLE 3

Aluminum sphere diameter (mm) that most closely emulates the coupling observed for the threat-object exemplars for the given orientation and for the different configuration and operation of test coils.

Threat Object Exemplar	Orientation	120 mm, 5 kHz	120 mm, 1 MHz	200 by 20 mm, 5 kHz	200 by 20 mm, 1 MHz
Handgun, Al	Max	90	100	100 ^a	100 ^a
Handgun, Al	Min	35	35	30	30
Handgun, Zn	Max	90	100	100 ^a	100 ^a
Handgun, Zn	Min	30	35	25	30
Knife, Al	Max	35	45	60	90
Knife, Al	Min	14	15	10	10
Knife, SS	Max	3 ^b	45	6 ^b	70 ^b
Knife, SS	Min	3 ^b	15	3 ^b	14 ^b
22 caliber cartridge	Max	7	16	5	16
22 caliber cartridge	Min	4	7	3 ^c	6
Pen refill	Max	3 ^c	10	3 ^c	11
Pen refill	Min	3 ^c	4	3 ^c	4

Note: ^a Indicates that inductance change with largest sphere was smaller than the change produced by the threat object exemplar. ^b Indicates a steel sphere was used to emulate the behavior of the nonferromagnetic test object ^c Indicates that the inductance change was smaller than could be measured with this coil, frequency, and instrument combination.

TABLE 4

Steel sphere diameter (mm) that most closely emulates the coupling observed for the threat-object exemplars for the given orientation and for the different configuration and operation of test coils.

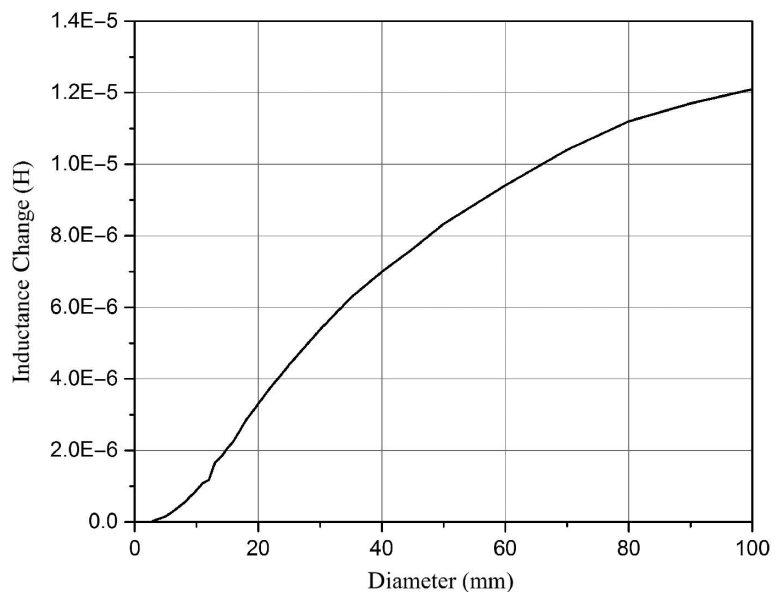
Threat Object Exemplar	Orientation	120 mm, 5 kHz	120 mm, 1 MHz	200 by 20 mm, 5 kHz	200 by 20 mm, 1 MHz
Handgun	Max	100 ^a	70	100	100 ^a
Handgun	Min	30	25	30	24
Knife	Max	100	40	100	60
Knife	Min	22	15	20	16
Handcuff key	Max	16	15	20	18
Handcuff key	Min	9	10	11	10
Screwdriver bit	Max	16	14	1	15
Screwdriver bit	Min	9	8	11	8
Razor blade	Max	13	16	13	20
Razor blade	Min	6	8	7	9

Note: ^a Indicates that inductance change with largest sphere was smaller than the change produced by the threat object exemplar.

value of the threat-object exemplar for its given orientation and for the configuration and operation of the test coils. The material for the sphere, steel or aluminum, that was selected to represent the threat-object exemplar was based on the sign of the change in frequency between the reference measurement and that for threat-object exemplar for the particular coil geometry and resonant frequency combination. An interesting result was obtained for the stainless steel knife threat object exemplar. The stainless steel selected for this threat object exemplar is non-ferromagnetic, but three of the four coil/frequency combinations yielded a change in frequency similar to the ferromagnetic materials. Fig. 3 plots the measured inductance change for the set of aluminum spheres using a 20-mm-diameter coil operated at 56 kHz.

FIG. 3

Inductance change for the set of aluminum spheres using a 20-mm-diameter coil operated at 56 kHz.



When a test object is positioned near the coil, the intercepted magnetic field lines cause a change in the inductance of the coil and thus, a change in the resonant frequency of the LC tank circuit.

Magnetic anisotropy was checked by measuring the 100-mm-diameter steel sphere versus rotation in two directions. A variation in inductance of approximately 15.9 % was noted. These measurements were performed using the 200-mm-by-200-mm coil operating at 5 kHz. This measurement was repeated on another date, and a similar result obtained (14.5 % variation). The 100-mm-diameter steel sphere was also checked for magnetic anisotropy using the 200-mm-by-200-mm coil at 1.04 MHz. The variation in inductance was approximately 0.06 %. The 90-mm-diameter steel sphere was checked for magnetic anisotropy using the 20-mm-by-50-turn coil operating at 58 kHz. A 2.5 % maximum variation was found. No magnetic anisotropy was observed for the 100-mm-diameter aluminum sphere.

Metal spheres used in this study were not large enough (diameter less than or equal to 100 mm) to emulate the electromagnetic signature of the larger threat-object exemplars at their orientation giving the largest detectability. This result is not surprising when comparing the geometries of the threat-object exemplars to that of the spheres and considering how the generated magnetic fields change with distance.

The measurements reported here have a number of sources of uncertainty. Each inductance value, L , reported is the mean of at least ten measurements; these were typically acquired in a 30-minute interval. The standard deviation (or standard uncertainty) of these ten measurements, σ_L , is the largest contributor to the measurement uncertainty, and its largest value was about 0.1 L , but the vast majority are less than 0.001 L . Day to day repeatability was also checked and found to be similar to the standard deviation of a block of ten measurements. The calibration of the frequency counter is not a contributor because the measurements were relative, each measurement result being the difference of two frequency measurements. In this case, only the short-term stability of the frequency counter contributes to the uncertainty. This stability is specified as 0.006 % and is a result of the laboratory temperature stability. Rearranging (4) to compute L , we get:

$$L = \frac{1}{4\pi^2 f^2 C}. \quad (5)$$

The uncertainty, u_L , in the measured inductance, L , using the method of LPU, can be estimated using:

$$u_L = \sqrt{\left(\frac{2}{4\pi^2 f^2 C} \frac{u_f}{f}\right)^2 + \left(\frac{1}{4\pi^2 f^2 C} \frac{u_c}{C}\right)^2 + \sigma_L^2} \quad (6)$$

The short-term stability of the capacitance (30-minute interval) would contribute to the uncertainty, u_C . The capacitors used were X7R or C0G rated, so that near room temperature, their capacitance change with temperature is about 3 % per °C. Because the change in temperature during a batch of 10 measurements was always less than 0.2°C, the maximum possible change in capacitance is 0.6 % during the measurement period. The frequency uncertainty, u_f , and the capacitance uncertainty, u_C , are very small compared to σ_L , so that we can conclude that u_L is dominated by σ_L and that u_L is at most 10 % of the inductance value for a couple of measurements but much lower in most cases.

TABLE 7

Alarm indication for aluminum spheres of different diameters at a test separation distance of nominally 80 mm.

	Sphere, aluminum (UNS A96061), nominal diameter (mm)		
	60	50	40
HHMD			
HHMD1	Yes	Yes	Yes
HHMD2	No	No	No
HHMD3	Yes	Yes	Yes
HHMD4	Yes	Yes	Marginal
HHMD5	Yes	Yes	Yes

TABLE 8

Alarm indication for steel spheres of different diameters at a test separation distance of nominally 80 mm.

	Sphere, steel (UNS G10180), nominal diameter (mm)				
	40	35	30	25	22
HHMD					
HHMD1	Yes	Yes	Yes	Yes	Yes
HHMD2	No	No	No	No	No
HHMD3	Yes	Yes	Yes	Yes	Yes
HHMD4	Yes	Yes	Yes	Yes	Marginal
HHMD5	Yes	Yes	Yes	Yes	Yes

Several different diameter spheres were examined at a test separation distance of nominally 80 mm. This test separation distance was chosen because (a) it was close in value to the current test separation distance developed by the practitioners and (b) provided slightly closer examination, which is more representative of field practice than the larger test separation distance. **Tables 7 and 8** present the results.

The HHMD4 exhibited marginal detection for (a) the nonferromagnetic (zinc and aluminum) handgun exemplars at the nominal 90-mm test separation distance and (b) the 40-mm-diameter sphere with a test separation distance of nominally 80 mm. Consequently, this diameter of sphere at this test separation distance emulates the detection results for the nonferromagnetic handgun exemplars.

All of the HHMDs could detect the ferromagnetic handgun exemplar at a nominal 90-mm-test separation distance. The HHMD4 did present a marginal detectability for the 22-mm-diameter steel sphere at a test separation distance of nominally 80 mm. This indicates the 22-mm-diameter steel sphere is too small and consequently, the 25-mm-diameter steel sphere is the most suitable to replace the ferromagnetic handgun test object.

The recommendations for the large-size object category are the 40-mm-diameter aluminum sphere and the 25-mm-diameter steel sphere at 80-mm test separation distance.

MEDIUM-SIZE TEST OBJECTS

Table 9 shows the detectability of the five HHMDs to the medium size test objects at the test separation distance of nominally 50 mm.

Several different diameter spheres were examined at a test separation distance of nominally 40 mm. This test separation distance was chosen because (a) it was close in

TABLE 9

Alarm indication for indicated medium-size test objects.

HHMD	Threat Object	
	Knife, Al (UNS A95052)	Knife, steel (UNS G41300)
HHMD1	Yes	Yes
HHMD2	No	Yes
HHMD3	Yes	Yes
HHMD4	Marginal	Yes
HHMD5	Yes	Yes

TABLE 10

Alarm indication for aluminum spheres of different diameters at a test separation distance of nominally 40 mm.

HHMD	Sphere, aluminum (UNS A96061), nominal diameter (mm)	
	18	15
HHMD1	Yes	Yes
HHMD2	No	No
HHMD3	Yes	Yes
HHMD4	Yes	Marginal
HHMD5	Yes	Yes

TABLE 11

Alarm indication for aluminum spheres of different diameters at a test separation distance of nominally 40 mm.

HHMD	Sphere, steel (UNS G10180), nominal diameter (mm)	
	12	10
HHMD1	Yes	Yes
HHMD2	Yes	No
HHMD3	Yes	Yes
HHMD4	Yes	Yes
HHMD5	Yes	Yes

value to the current test separation distance developed by the practitioners and (b) provided slightly closer examination, which is more representative of field practice, for this threat size, than the 50-mm test separation distance. The results are shown in [Tables 10](#) and [11](#).

The HHMD4 exhibited marginal detection for the nonferromagnetic (zinc and aluminum) knife exemplars at 50-mm test separation distance and also for the 15-mm-diameter sphere with a test separation distance of 40 mm. The HHMD2 could not detect the knife exemplar or the spheres. Consequently, the 15-mm-diameter sphere at this test separation distance emulates the detection results for the nonferromagnetic handgun exemplars.

All of the HHMDs could detect the ferromagnetic knife exemplar at a nominal 50-mm test separation distance. The HHMD2 did not detect the 10-mm-diameter steel sphere at a nominal 40-mm test separation distance, indicating that this diameter is too small to represent the knife exemplar.

The recommendations for medium-size object category are the 15-mm-diameter aluminum sphere and the 12-mm-diameter steel sphere at 40-mm test separation distance.

SMALL-SIZE TEST OBJECTS

Table 12 shows the detectability of the five HHMDs to the small size test objects at the test separation distance of nominally 30 mm.

Several different diameter spheres were examined at a test separation distance of nominally 20 mm. This test separation distance was chosen because (a) it was close in value to the current test separation distance developed by the practitioners and (b) provided slightly closer examination, which is more representative of field practice for this threat size than the 30-mm test separation distance. See **Tables 13** and **14**.

The HHMD4 exhibited marginal detection for the nonferromagnetic (nonferromagnetic stainless steel knife and lead portion of the 22-caliber cartridge) exemplars at the 30-mm test separation distance and the 8-mm- and 9-mm-diameter steel spheres at a test separation distance of 20 mm. The HHMD2 could detect the stainless-steel knife exemplar but not the 22-caliber cartridge exemplar. The HHMD2 could detect the 9-mm-diameter aluminum sphere but not the 8-mm-diameter sphere. Consequently, the 9-mm-diameter of sphere at this test separation distance emulates the detection results for the nonferromagnetic exemplars.

TABLE 12

Alarm indication for indicated small-size test objects.

HHMD	Threat Object			
	#2 Phillips bit, steel (UNS G41400)	Handcuff key, steel (UNS G10180)	Knife, SS (UNS S30400)	22 cal round* (UNS L50045)
HHMD1	Yes	Yes	Yes	Yes
HHMD2	Yes	Yes	Yes	No
HHMD3	Yes	Yes	Yes	Yes
HHMD4	Yes	Yes	Marginal	Marginal
HHMD5	Yes	Yes	Yes	Yes

Note: *Lead part was closest to metal detector.

TABLE 13

Alarm indication for aluminum spheres of different diameters at a test separation distance of nominally 20 mm.

HHMD	Sphere, aluminum (UNS A96061), nominal diameter (mm)	
	9	8
HHMD1	Yes	Yes
HHMD2	Yes	No
HHMD3	Yes	Yes
HHMD4	Marginal	Marginal
HHMD5	Yes	Yes

TABLE 14

Alarm indication for aluminum spheres of different diameters at a test separation distance of nominally 20 mm.

	Sphere, steel (UNS G10180), nominal diameter (mm)		
	7	6	5
HHMD			
HHMD1	Yes	Yes	Yes
HHMD2	Yes	No	No
HHMD3	Yes	Yes	Yes
HHMD4	Yes	Yes	marginal
HHMD5	Yes	Yes	Yes

All of the HHMDs could detect the ferromagnetic small-size exemplars at a nominal 30-mm test separation distance. The HHMD2 did not detect the 6-mm-diameter or 5-mm-diameter steel spheres at a nominal 20-mm test separation distance, and the HHMD4 demonstrated marginal detection of the 5-mm-diameter sphere. This indicates that the 7-mm-diameter steel sphere best represents the small-size ferromagnetic test objects.

The recommendations for the small-size object category are the 9-mm-diameter aluminum sphere and the 7-mm-diameter steel sphere at a test separation distance of 20 mm.

VERY SMALL SIZE TEST OBJECTS

Table 15 shows the detectability of the five HHMDs to the very small size test objects at the test separation distance of nominally 10 mm.

Several different diameter spheres were examined at a test separation distance of nominally 5 mm. This test separation distance was chosen because (a) it was close in value to the current test separation distance developed by the practitioners and (b) provided slightly closer examination, which is more representative of field practice, for this threat size, than the 10-mm test separation distance. The results are shown in Tables 16 and 17.

All HHMDs could detect the nonferromagnetic test object at a test separation distance of nominally 10 mm as well as the 6-mm-diameter aluminum spheres at a test separation distance of nominally 5 mm. The HHMD4 could not detect the 5-mm-diameter aluminum sphere at a test separation distance of about 5 mm. Consequently, the 6-mm-diameter aluminum sphere at the test separation distance of 5 mm emulates the detection results for the very-small-size exemplars at a test separation distance of nominally 10 mm.

TABLE 15

Alarm indication for indicated very-small-size test objects.

HHMD	Threat Object	
	Pen refill, brass (UNS C36000)	Disposable razor blade, steel (UNS G10100)
HHMD1	Yes	Yes
HHMD2	Yes	No
HHMD3	Yes	Yes
HHMD4	Yes	Marginal
HHMD5	Yes	Yes

TABLE 16

Alarm indication for aluminum spheres of different diameters at a test separation distance of nominally 5 mm.

	Sphere, aluminum (UNS A96061), nominal diameter (mm)	
	6	5
HHMD		
HHMD1	Yes	Yes
HHMD2	Yes	Yes
HHMD3	Yes	Yes
HHMD4	Yes	Marginal
HHMD5	Yes	Yes

TABLE 17

Alarm indication for aluminum spheres of different diameters at a test separation distance of nominally 5 mm.

	Sphere, steel (UNS G10180), nominal diameter (mm)		
	5	4	3
HHMD			
HHMD1	Yes	Yes	No
HHMD2	Yes	Yes	No
HHMD3	Yes	Yes	Yes
HHMD4	Yes	Marginal	No
HHMD5	Yes	Yes	No

The HHMD2 could not detect the disposable razor blade exemplar, and the HHMD4 demonstrated marginal detector performance for this test object at a test separation distance of 10 mm. All HHMDs could detect the 5-mm-diameter and 4-mm-diameter steel spheres at a nominal test separation distance of 5 mm, although the HHMD4 was marginal. Only one HHMD could detect the 3-mm-diameter steel sphere at a nominal 5-mm test separation distance. This indicates that the 4-mm-diameter steel sphere best represents the very-small-size ferromagnetic test objects.

The recommendations for the very-small-size object category are the 6-mm-diameter aluminum sphere and the 4-mm-diameter steel sphere at a test separation distance of 5 mm.

Conclusion

The detection performance of HHMDs and HWMDs to a given threat-object exemplar is dependent on its orientation relative to the metal-detector-generated magnetic field, thus impacting the accuracy and reproducibility of detection performance testing and comparison. Spherical test objects were suggested to avoid this orientation-induced measurement error. Numerical simulations showed that the threat-object exemplar, for a given orientation, can be replaced by a spherical test object. These results were experimentally validated using a custom build measurement setup. A comparison of the detectability of threat-object exemplars to spherical test objects using five commercially available HHMDs identified the sphere diameters and test separation distances that emulate a threat-object exemplar at its minimum orientation condition and the given test separation

distance. This information will be used to make recommendations for inclusion of the spherical test object in the under-development ASTM standard.

References

- [1] Paulter, N. G., Jr., Larson, D. R., and Ely, J. A., “Test Object for Accurate and Reproducible Measurement of the Detection Response of Hand-worn and Hand-held Metal Detectors,” *J. Res. Nat. Inst. Stand. Technol.*, Vol. 121, 2016, pp. 401–419, <https://perma.cc/DN8X-H8WH> (accessed 27 March 2018).
- [2] Joint Committee for Guides in Metrology, *Evaluation of Measurement Data— Guide to the Expression of Uncertainty in Measurement*, Joint Committee for Guides in Metrology, 2008, 134p, <https://perma.cc/2AK3-RJXC> (accessed 27 March 2018).
- [3] Osborn, J. A., “Demagnetizing Factors of the General Ellipsoid,” *Phys. Rev.*, Vol. 67, Nos. 11–12, 1945, pp. 351–357, <https://doi.org/10.1103/PhysRev.67.351>
- [4] Chen, D.-X., Brug, J. A., and Goldfarb, R. B., “Demagnetizing Factors for Cylinders,” *IEEE Trans. Magn.*, Vol. 27, No. 4, 1991, pp. 3601–3619, <https://doi.org/10.1109/20.102932>
- [5] Aharoni, A., “Demagnetizing Factors for Rectangular Ferromagnetic Prisms,” *J. Appl. Phys.*, Vol. 83, No. 6, 1998, pp. 3432–3434, <https://doi.org/10.1063/1.367113>
- [6] NIJ Standard 0602.02, *Hand-Held Metal Detectors for Use in Concealed Weapon and Contraband Detection*, National Institute of Justice, Washington, DC, 2003, <https://nij.gov/>
- [7] ASTM F3020-16, *Performance Standard for Hand-Worn Metal Detectors Used in Safety and Security*, ASTM International, West Conshohocken, PA, 2016, www.astm.org
- [8] Janezic, M. D., Kaiser, R. F., Baker-Jarvis, J., and Free, G., “DC Conductivity Measurements of Metals,” *NIST Technical Note 1531*, National Institute of Standards and Technology, Washington, DC, 2004, 24p, <https://doi.org/10.6028/NIST.TN.1531>
- [9] Janezic, M. D. and Baker-Jarvis, J., “Relative Permeability Measurements for Metal-Detector Research,” *NIST Technical Note 1532*, National Institute of Standards and Technology, Washington, DC, 2004, 20p, <https://doi.org/10.6028/NIST.TN.1532>
- [10] Thompson, D. O. and Chimenti, D. E., Eds., *Review of Progress in Quantitative Nondestructive Evaluation*, Vol. 25A, American Institute of Physics, College Park, MD, 2006.
- [11] Wilson, N. and Bunch, P., “Magnetic Permeability of Stainless Steel for Use in Accelerator Beam Transport Systems,” presented at the *IEEE Particle Accelerator Conference*, San Francisco, CA, May 6–9, 1991, IEEE, New York, NY, pp. 2322–2324.
- [12] Hoburg, J. F., Fugate, D. W., Clairmont, B. A., and Lordan, R. J., “Comparisons of Measured and Calculated Power Frequency Magnetic Shielding by Multilayered Cylinders,” *IEEE Trans. Power Delivery*, Vol. 12, No. 4, 1997, pp. 1704–1710, <https://doi.org/10.1109/61.634194>